Minimizing Energy Consumption of Elastic Robots in Repetitive Tasks

Alexandra Velasco Vivas, Antonello Cherubini, Manolo Garabini, *Member, IEEE*, Paolo Salaris, and Antonio Bicchi

***Abstract*—Energy consumption is an important issue in robotics. This article deals with the problem of reducing the energy consumption of compliant electro-mechanical systems while performing periodic tasks. After deriving performance indices to quantify the energy consumption of a mechanical system, we propose a method to determine both the optimal compliant actuation parameters, and link trajectories to minimize energy consumption. We show how this problem can be cast in a simpler one where the optimization regards only parameters that define the shape of periodic trajectories to be subsequently determined by using numerical optimization tools. Indeed, in our framework, the optimal stiffness and spring preload can be analytically obtained as a function of the desired link trajectories. We then provide simulations and experimental validations of the obtained results on a two-link compliant manipulator platform which performs a repetitive pick-and-place task. Our experiments show that the use of compliant actuators instead of rigid ones and the optimization of their compliant parameters give rise to an energy saving up to 62% with respect to rigid actuation. Moreover, the simultaneous optimization of the compliant parameters and link trajectories provide an additional energy saving up to 20%.**

***Index Terms*—Compliant actuation, elastic robots, energy saving, parallel elastic actuators (PEAs), series elastic actuators (SEAs), stiffness optimization, trajectory optimization.**

I. Introduction

ENERGY efficiency is a fundamental issue on a global scale, and it plays a key role in the Sustainable Development Goals of the UN2030 Agenda [1]. The reduction of energy consumption is vital in many aspects of our daily life and is also a relevant topic in the manufacturing industry and in robotics [2], [3]. It is, especially, relevant when considering autonomous electro-mechanical systems that perform repetitive movements such as pick-and-place tasks in industrial environments. The reduction of energy consumption of mechanical systems can be achieved by using one or a combination of different strategies, e.g., by properly designing the mechanical structure and the actuators (see [4], [5], [6]), controllers (see [7], [8]), and trajectories (see [9], [10], [11]). Indeed, actuators are crucial components that dramatically affect the performance of robots.

Developments in this field have introduced fixed or physically adjustable compliant elements to enrich the dynamics of conventional motors. These devices provide advantages w.r.t. rigid actuators, including higher peak torque, higher peak speed, lower energy consumption, and improved safety (see [12], [13]). This tendency is the so-called elastic actuation, used for instance in manipulation [14], or in humanoid design [15].

Among elastic actuators, two important categories are parallel elastic actuators (PEAs) and series elastic actuators (SEAs). PEAs have an elastic element in parallel with the motor (i.e., between two links) [16], while SEAs have a linear compliant element between a high-impedance actuator and the load.

Other examples of soft actuators are variable stiffness actuators (VSAs) that have mechanically adjustable stiffness, and variable impedance actuators (VIAs) that have brakes or dampers to adjust the impedance [17]. Recent studies explore the role of such devices to enhance performance, in highly dynamic tasks. For instance, Park et al. [18] and Garabini et al. [19] presented a method to optimally choose the stiffness to maximize the velocity of a VSA at a given final position with free final time.

Recent studies analyzed the efficiency of PEAs and SEAs in sinusoidal trajectories, showing that, when properly tuned, such devices allow significant energy savings, ranging between 20% and 78%, with respect to a rigid actuation [20]. Moreover [21] shows that, when studying PEAs and SEAs, a dynamic model of the motor is key to accurately predicting the power consumption of the actuation system.

Energy efficiency using PEAs is also specifically evaluated in [22], where authors study the effects of passive joint stiffness in the hip and knee of a biped robot. In a similar way, Schauss et al. [23] introduced the effects of stiffness in the ankle to reduce energy consumption on bipedal

Manuscript received 6 December 2022; accepted 8 March 2023. Date of publication 7 April 2023; date of current version 19 July 2023. This work was supported in part by EC through "DARKO," Dynamic Agile Production Robots That Learn and Optimize Knowledge and Operations under Grant 101017274 and through "NI," Natural Intelligence under Grant 101016970; and in part by the Italian Ministry of Education and Research (MIUR) in the framework of the FoReLab and CrossLab project (Departments of Excellence). This article was recommended by Associate Editor C. Yang. *(Corresponding author: Manolo Garabini.)*

Alexandra Velasco Vivas is with the Mechatronics Department, Universidad Militar Nueva Granada, Bogotá 110111, Colombia, and also with the Centro di Ricerca "E. Piaggio," University of Pisa, 56122 Pisa, Italy.

Antonello Cherubini is with the Department of Industrial Engineering, University of Trento, 38122 Trento, Italy and also with the Centro di Ricerca "E. Piaggio," University of Pisa, 56122 Pisa, Italy.

Manolo Garabini and Paolo Salaris are with the Centro di Ricerca "E. Piaggio," University of Pisa, 56122 Pisa, Italy (e-mail: manolo.garabini@unipi.it).

Antonio Bicchi is with the Centro di Ricerca "E. Piaggio," University of Pisa, 56122 Pisa, Italy, and also with the Adv. Robotics, Istituto Italiano di Tecnologia, 16163 Genoa, Italy.

Color versions of one or more figures in this article are available at https://doi.org/10.1109/TSMC.2023.3260644.

Digital Object Identifier 10.1109/TSMC.2023.3260644

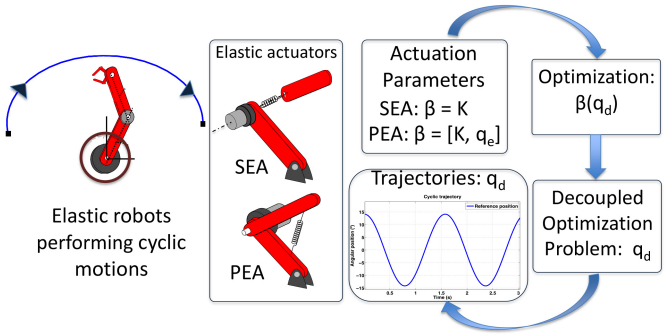

Fig. 1. Compliant mechanical systems with SEAs and PEAs in repetitive tasks. In our framework, the minimization of the energy consumption in terms of compliant parameters β and link trajectories q_d can be decoupled: we first obtain an analytical expression of the compliant parameters as a function of the link trajectories ($\beta(q_d)$) and then, we determine, by using numerical optimization tools, the optimal link trajectories q_d^*.

locomotion. Additionally, Yesilevskiy et al. [24] evaluated the energy consumption of PEAs and SEAs in a hopping motion. Moreover, in [25] the energy efficiency of VSAs is evaluated. Finally, Scheint et al. [26] addressed the role of compliance in walking controller synthesis and carry out the simultaneous optimization of the gait and leg spring stiffness for a biped that uses PEAs, as well as the optimization of the gait at a fixed leg spring stiffness. The latter work does not address the SEAs case.

This article aims at exploring the use of compliant actuators to enhance the performance of mechanical systems. In particular, our objective is to determine compliant parameters of PEAs and SEAs, i.e., stiffness, spring preload, and the link trajectories to perform repetitive/periodic motions with minimum energy consumption (see Fig. 1).

In the literature, several approaches try to find compliant parameters and link trajectories with minimum energy consumption. However, a methodology that recast the optimization problem in order to determine how to tune simultaneously soft actuation and to select the link trajectories for reducing the energy consumption of mechanical systems is still missing.

Typically the aforementioned problems are separately tackled. Regarding trajectory optimization (or optimal control) alone, there is a comprehensive literature body that spans from minimum-time problems to efficiency maximization. Several works have been proposed in this regard. For instance, Consolini et al. [27], [28] presented a globally optimal feedforward control technique that allows a Flexible-Joint Robot to perform a smooth rest-to-rest motion and to remove the link oscillations, by leveraging a linear programming approach. A similar bang-bang regulation controller is proposed in [29], in which the problem is recast into a two-body mechanical problem, while vibrations suppression via an optimization technique is achieved in [30]. Other numerical solutions that deal with the time-optimal trajectory planning problem are in [31], where the SEA case is analyzed and in [32] and [33] for the VSA-adj category. The latter exploits an iterative linear quadratic regulator (iLQR) approach. Moreover, solutions are given in [34], for the VSA case. The same problem is analyzed in [35] for a different actuator concept, in which the offline-generated trajectories are embedded into principal components (PCs) to be reused online with a reduced computational cost. On the other hand, to the best of our knowledge, the problem of parameter optimization alone has been analyzed for few specific cases. For example, the stiffness value to reduce the energy consumption of a biped running robot is addressed in [36], where the authors tune the optimal stiffness for an SEA without optimizing the trajectory.

Regarding the simultaneous design of the robot trajectories and the springs, Schmit and Okada [37] presented a method to minimize the actuator torques in the case of PEAs. Similarly to our proposal, the optimization problem is treated as a trajectory optimization problem. This approach is extended in [9], where optimal control theory is used to find the trajectories for PEA robots that work in production lines. This work is different from our methodology in that the authors find trajectories by inverse dynamics, and then they obtain the optimal spring force profile. In addition to compliant electromechanical systems, the proposed optimization method can also be applied to improve the performance of other parallel elastic concepts, e.g., some passive exoskeletons [38].

A. Contribution of This Article

In [39] we investigated the optimization of the stiffness and preload of PEAs and SEAs in fully actuated and underactuated mechanical systems without, first, providing a clear relationship between the performance indices that we considered and the actual energy consumption and, second, solving the relevant problem of concurrently optimizing stiffness/preload and periodic link trajectories parameters.

In this article, after recalling the cost indexes to be optimized (that have been already introduced in [39]), we discuss better the physical relation between these cost indices and the energy consumption of a robot powered by electrical motors (Section III). Then, we present the methodology that allows to obtain beforehand the analytic expression of the optimal compliant parameters in terms of generic link trajectories (already proposed in [39]), and we extend this methodology in order to cast the overall optimization problem in a simpler one where *only* the parameters that define the optimal periodic link trajectories should be optimized (Section V). More specifically, we express the optimal control problem in the classical Bolza form, and the trajectory parameters are subsequently obtained by applying numerical optimization tools. We apply our methodology to a two-link manipulator actuated by SEAs both in simulation and experiments, the latter on a 2 degrees of freedom (DoF) manipulator prototype (Section VI). We show that the use of optimal stiffness allows an energy saving up to 62% w.r.t. rigid actuation. On the other hand, by concurrently optimizing the trajectories and the actuation parameters, an additional energy saving of at least 20% is achieved.

This article is structured as follows: in Section II the optimal control problem is stated. In Section III, we derive a realistic measurement of the energy consumption of a system and we propose two performance indices which allow to find an analytical solution to our problem, providing their relationship with the realistic energy consumption. In Section IV,

the optimal value of the compliant parameters in analytic form is obtained as a function of the link trajectories. Then, in Section V, the optimization problem is reformulated only in terms of the link trajectories in a standard form and in Section VI an example in the standard form is optimized with the numerical optimization tool GPOPS-II in order to find the optimal parameters that define the periodic link trajectories. Finally, in Section VII experimental results for that example are also reported, while Section VIII concludes this article.

II. Problem Statement

In this section, we show the different mechanical systems considered in this article and their dynamical models, and we state the optimization problem as in [39]. We refer to the following definitions: mechanical systems can be *fully actuated* if it is possible to control the acceleration of each DoF [40], or *underactuated* if there are less control inputs than DoF [41]. Moreover, depending on how and where the springs are placed in the system, the dynamics of a mechanical system can assume particular forms. The method proposed in this article is general enough to be applied to n-DoF systems that use compliant actuation with nonlinear and nondiagonal stiffness matrix. Nonetheless, we will first analyze the case with linear and diagonal stiffness matrices to gain an insight and clarify the matter.

A. Mechanical Systems With PEAs and SEAs

Let us consider an underactuated compliant mechanical system actuated by PEAs. Indicating by $q \in \Re^n$ and $z \in \Re^m$ the actuated and the nonactuated generalized coordinates, respectively, and by $\tau \in \Re^n$ the generalized torque provided by actuators, the dynamics can be written as follows:

$$f_u(\ddot{z}, \dot{z}, z, \ddot{q}, \dot{q}, q, t) = 0 \tag{1}$$

$$f_a(\ddot{z}, \dot{z}, z, \ddot{q}, \dot{q}, q, t) = -K(q_e - q) + \tau \tag{2}$$

where $q_e \in \Re^n$ is the spring preload and $K \in \Re^{n\times n}$ is the stiffness matrix. The terms f_u and f_a include inertia, coriolis, and gravity terms.

In case the system is fully actuated the dynamics can be written as follows:

$$f(\ddot{q}, \dot{q}, q, t) = K(q_e - q) + \tau. \tag{3}$$

Notice that by integration of (1) it is possible to find z as a function of the desired trajectories $q_d(t)$. Hence, by substituting z in (2), we can obtain equations in the form of (3) where q_d takes the place of q. Therefore, analyzing systems that are fully actuated also covers the cases of mechanical systems that are underactuated. Notice that the transformation of (1) and (2) into (3) by the integration of (1) may ignore possibly unstable zero dynamics. However, this is not discussed further in this article since in the next sections we will refer to PEAs and SEAs. Parallel elastic actuation does not change the size of the state of the system, and, hence, it cannot lead to zero dynamics. In principle SEAs could lead to zero dynamics, however, flexible joint robots are completely feedback linearizable as shown in [42].

Consider now an underactuated mechanical system actuated by SEAs with the following dynamics[1]:

$$f_u(\ddot{z}, \dot{z}, z, \ddot{q}, \dot{q}, q, t) = 0 \tag{4}$$

$$f_a(\ddot{z}, \dot{z}, z, \ddot{q}, \dot{q}, q, t) = -K(q - \theta) \tag{5}$$

$$J_m\ddot{\theta} = K(q - \theta) + \tau \tag{6}$$

where $\theta \in \Re^n$ is the vector of the motor positions and J_m is the inertia matrix of the motors. The use of SEAs instead of PEAs increases the number of DoFs, which become $2n$, while the control inputs remain n. In case the system is fully actuated the dynamics become

$$f(\ddot{q}, \dot{q}, q, t) = -K(q - \theta) \tag{7}$$

$$J_m\ddot{\theta} = K(q - \theta) + \tau. \tag{8}$$

Notice also, here, that by integration of (4) it is possible to find $z(q_d)$ and that, by substituting z in (5), we can obtain equations in the form (7) where q_d takes the place of q. Thus, analyzing systems that have 1 SEA for each DoF [as in (7) and (8)] also covers the cases of mechanical systems that are further underactuated with SEAs as in (4)–(6).

B. Optimization Problem

In this article, we consider the problem of determining the optimal stiffness $\hat{K}$ and/or preload $\hat{q}_e$, as well as optimal link trajectories $\hat{q}(t)$, such that the cost functional J_i is minimized, i.e., the following optimization problem:

$$\min_{\tau(t),\beta,q(t)} J_i(q, \dot{q}, \ddot{q}, \beta(q)), \qquad i \in \{1, 2\}$$

$$\text{s.t.} \begin{cases} \text{Dynamics equations} \\ q(t) = q(t + T) \\ \xi_1(q, \dot{q}, \ddot{q}) \le 0 \\ \xi_2(q, \dot{q}, \ddot{q}) = 0 \\ \beta_m \le \beta \le \beta_M \end{cases} \tag{9}$$

where the term *Dynamics equations* corresponds to (3) or both (7) and (8), depending on the actuation case. J_i is a cost functional based on the energy consumption that will be analyzed in the following section. β is a vector containing, in case of PEAs, both joint stiffness K and preload q_e with limits $\beta_M = [K_M, q_{e,M}]$ and $\beta_m = [K_m, q_{e,m}]$; or, in case of SEAs, only stiffness K with limits $\beta_M = K_M$ and $\beta_m = K_m$. Finally, the nonlinear constraints ξ_1 and ξ_2, which depend on the variables q, $\dot{q}$, and $\ddot{q}$, define the task. For instance, in a pick-and-place task, we constrain the motion of the end-effector to the line between two specific points.

III. Physical Relevance of Performance Indices

The indices proposed in this work allow us to find an analytical solution to the optimization problem and are related to the energy consumption of a system. In this section, we derive first an index that gives a realistic measurement of a mechanical system's energy consumption. Then we propose two indices

[1] Viscous friction term is not written to make analytical calculations simpler. Adding the corresponding term does not change the procedure. In the experimental tests presented in this article, viscous friction is indeed considered.

that allow us to solve the problem analytically, and finally, we present their relation with the energy measurement of the system.

A. Energy Consumption Index With Energy Recovery

For simplicity, consider an actuation system based on dc electric motors, each of which can be modeled as follows:

$$\begin{aligned} v(t) &= R\,i(t) + L\,\frac{d\,i(t)}{dt} + K_I\,\omega(t) \\ \tau(t) &= K_I\,i(t) \end{aligned} \tag{10}$$

where $v(t)$ is the input voltage, $i(t)$ is the absorbed current, R, L, and K_I are the motor internal resistance, inductance, and torque factor (to ease the notation, the torque and speed constants are both considered equal to K_I), $\tau(t)$ is the torque and $\omega(t)$ is the output shaft speed. Notice that $\omega(t)$ can be either $\dot{q}(t)$ for a joint actuated with PEA, or $\dot{\theta}(t)$ for a joint actuated with SEA.

Considering a cyclic trajectory, for which $i(t) = i(t+T)\forall t$, it holds that $\int_0^T L\,(di/dt)i(t)\,dt = (1/2)\,L\,i(t)^2|_0^T = 0$, thus

$$\begin{aligned} E &= \int_0^T v\,i\,dt = \int_0^T \left(R\,i^2 + L\,\frac{di}{dt}i + K_I\,\omega\,i\right)dt \\ &= \int_0^T R\,i^2 dt + \int_0^T K_I\,\omega\,i\,dt \end{aligned} \tag{11}$$

is the energy consumption of the system.

Due to the direct relation between current and torque, we can rewrite (11) as follows:

$$E = \gamma_e \int_0^T \tau^2(t)\,dt + \gamma_m \int_0^T \tau(t)\,\omega(t)\,dt \stackrel{def}{=} E_e + E_m \tag{12}$$

where γ_e is an experimental parameter, $\gamma_e = (R/K_I^2)$, $\gamma_m = 1$, and K_I can be obtained as the ratio between nominal torque and nominal current. We defined E_e as the integral of dissipated power inside the motor and E_m as the integral of mechanical power at the motor output.

B. Energy Consumption Index Without Energy Recovery

E_m can be positive when accelerating, or negative when braking.

If the motor could be used as a generator, without losses, (12) would be correct, but in most of the cases of interest this is not true. Thus, the definition (12) changes as follows.

Let $\eta \in [0 \div 1]$ be the efficiency of the motor energy recovery (zero if the motor cannot be used as a generator) and consider a function

$$\ell(x,\eta) = \begin{cases} x, & \text{if } x \geq 0 \\ \eta\,x, & \text{otherwise} \end{cases} \tag{13}$$

thus, we can define a new parameter, E_m, that is more accurate than the previously defined E_m

$$E_m = \int_0^T \ell(\tau(t)\,\omega(t),\eta)\,dt. \tag{14}$$

Equation (12) combined with (14) provides a realistic measure of the system energy. We can now write the index J_T, also considering the reduction ratio N at the motor side, such that

$$J_T = \gamma_e \int_0^T \frac{\tau^2(t)}{N^2}dt + \int_0^T \ell(\tau(t)\,\omega(t),\eta)dt. \tag{15}$$

Notice that when $\eta \neq 1$, using (15) as cost functional in the optimization problem does not lead to an analytical solution.

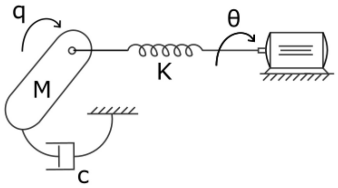

Fig. 2. Single joint system for the evaluation of the performance indices.

C. Performance Indices

We propose two cost functionals, namely, Squared Power J_1 and Squared Torque J_2, in order to find the values of the optimal joint stiffness $\hat{K}$ and preload $\hat{q}_e$ (the latter for PEAs), together with the optimal link trajectories $\hat{q}(t)$.

1) *Squared-Power Index:* Squared mechanical power over the n joints in a period T

$$J_1 = \sum_{j=1}^{n} \int_0^T \left(\tau_j(t)\omega_j(t)\right)^2 dt. \tag{16}$$

2) *Squared-Torque Index:* Square of the torque τ over the n joints in a period T

$$J_2 = \sum_{j=1}^{n} \int_0^T \tau_j^2(t)\;dt. \tag{17}$$

D. Relation of the Derived Index With the Proposed Performance Indices

Here, we present a detailed analysis to determine the relevance of the proposed indices J_1 and J_2 and their relation with J_T.

For the analysis, we consider a single joint linear system, as the one in Fig. 2, with inertia M, damping c, and stiffness K whose dynamics are described by $M\ddot{q} + c\dot{q} + K(q-\theta) = 0$. Assume that the desired link trajectory is given as a sinusoidal function of the form $q(t) = A\sin(\omega t)$, with A and ω the amplitude and the speed of the motion, respectively. The idea is to determine which of the proposed indices represents more accurately the behavior of the system's energy. With this aim, we compare in several cases, $\hat{K}$ and J_i from the solution of the problem (9) with the numerical solution of the problem using (15) as a reference for a realistic cost functional.

The results are shown in Fig. 3 where $\hat{K}_T$, $\hat{K}_1$, and $\hat{K}_2$ represent the optimal stiffness that is obtained by minimizing J_T, J_1, and J_2, respectively.

First, let us analyze the case of an ideal motor, where $\eta = 1$, i.e., energy is completely recovered when braking. In this case, the index J_2 based on the squared torque indicates better the real energy consumption of the system [i.e., $\hat{K}_2$ is equal to $\hat{K}_T(\eta = 1)$], regardless of the parameters c, ω, nor the gear reduction

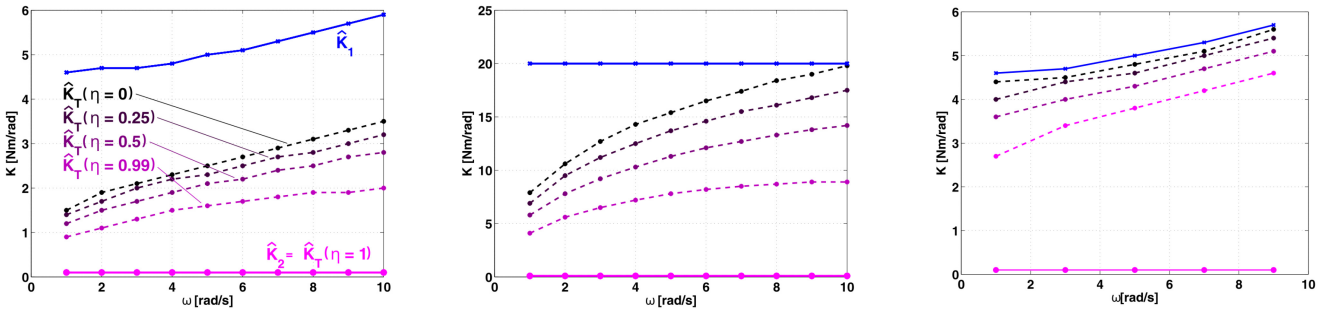

Fig. 3. Optimal stiffness varying the frequency ω and the efficiency η for different values of damping c and low reduction ratio N. K_1, K_2, and K_T denote, respectively, the optimal stiffness result using J_1, J_2, and the total energy in (15) (dashed lines). The simulation values for the single joint system are $M = 0.1$, $A = \pi/3$, $\omega \in [1, 10]$ rad/s, $\eta \in [0, 1]$. $\gamma_e = (R/K_I) = 3.8$, $R = 3.69\ \Omega$, $K_I = C_n/I_n$, $C_n = 0.84$, and $I_n = 0.87$. (a) Comparison using $N = 1$ and $c = 0.25$. (b) Comparison using $N = 1$ and $c = 1$. (c) Comparison using $N = 30$ and $c = 0.25$.

TABLE I
COST FUNCTIONS THAT BETTER REPRESENT THE BEHAVIOR OF ENERGY CONSUMPTION DEPENDING ON η AND N. WHERE $\star$ APPEARS, THE COST FUNCTION THAT BETTER REPRESENTS THE ENERGY CONSUMPTION CAN BE EITHER J_1 OR J_2, SO THE SPECIFIC CASE MUST BE ANALYZED

Damping c	Not Damped $c \to 0$		Damped	
η	$\to 0$	$\to 1$	$\to 0$	$\to 1$
$N \to 1$ (Low)	J_1	J_2	$\star$	J_2
N (High)	J_1	J_2	J_1	J_2

ratio N. The optimal stiffness obtained when minimizing J_2 (red continuous lines) is in all cases $\hat{K} = 0.1$ [Nm/rad].

Now, consider the case in which $\eta = 0$, i.e., the motor cannot be used as a generator. In this case, the system's parameters become more relevant to the discussion. In particular, we will focus on the effects of the link damping c and the reduction ratio N. With a high reduction ratio, it is better to use the index J_1 based on the mechanical power of the system. If the reduction ratio is low ($N \to 1$) and there is negligible damping, the best approach is still J_1; however, none of the indices predicts the energy consumption behavior when the system is damped. As observed, while the efficiency decreases, the results when using J_1 (blue lines) approximate better the behavior of the index given by the energy consumption of the system. Depending on the motor efficiency, the system's behavior is better described by J_1 or J_2, but the results may not coincide as in Fig. 3(a) and (b). On the other hand, Fig. 3(c) shows that in some cases, the behavior is more likely represented by the index J_1, unless the motor is ideal, i.e., $\eta = 1$. So, when $\eta = 1$, if there is no damping (or it is negligible) the term $\int_0^T \tau(t)\omega(t)dt$ becomes (almost) zero and the index is well represented by the term $\int_0^T \tau^2(t)dt$. If, on the other extreme, $\eta = 0$, the term $\int_0^T \ell(\tau(t)\,\omega(t), \eta)dt$ increases, and if N is high, the term $(\gamma_e/N^2)\int_0^T \tau^2 dt$ can be neglected. All the aforementioned cases are summarized in Table I.

IV. Optimization of Stiffness and Preload Parameters

We can now briefly recall the computation done in [39] where the optimal compliant actuation parameters of mechanical systems presented in Section II under the hypothesis that $K = \text{diag}[K_1, K_2, \ldots, K_n]$ and $J_m = \text{diag}[J_{m1}, J_{m2}, \ldots, J_{mn}]$ (which is valid for many mechanical systems) are derived. Velasco et al. [39] also showed that, once the optimal actuation parameters are obtained as a function of the chosen set of desired link trajectories $q_d(t)$, the problem of optimizing the actuation parameters and the link trajectories can be cast in a simpler problem where the optimization regards only the latter. However, the problem of finding optimal cyclic trajectories has not been solved in [39].

Regarding the optimal stiffness and preload parameters, for the case of PEAs, in [39] it has been shown that the optimal solution for each K_j is such that $(\partial J_{1,j}/\partial K_j) = 0$ and can be found by solving the equation: $4A_{S,j} + 3K_jB_{S,j} + 2C_{S,j}K_j^2 + D_{S,j}K_j^3 = 0$, where the value of the coefficients can be found in [39, Sec. III].

For the case of SEAs, the optimal solution for each K_j is such that $(\partial J_{2,j}/\partial K_j) = 0$ and

$$J_{2,j} = \frac{F_{S,j}}{K_j^2} + \frac{G_{S,j}}{K_j} + H_{S,j}, \qquad \hat{K}_j = -2\frac{F_{S,j}}{G_{S,j}} \tag{18}$$

$$F_{S,j} = \int_0^T \left(J_{m_j}\ddot{f}_j\right)^2 dt, \;\; H_{S,j} = \int_0^T \left(J_{m_j}\ddot{q}_{d,j} + f_j\right)^2 dt$$

$$G_{S,j} = \int_0^T 2J_{m_j}\ddot{f}_j\left(J_{m_j}\ddot{q}_{d,j} + f_j\right)dt$$

where $\ddot{f}_j$ and $\ddot{q}_{d,j}$ are the second time derivative of the jth component of f and q_d, respectively.

The optimal values of stiffness $\hat{K}_j$ may not necessarily be inside an admissible range of values. In this case, the optimal values will be on the boundary of the admissible set of values as described in [39, Sec. III].

V. Trajectory Optimization Problem

With the procedure followed so far, we can replace the optimal values of $\beta(q)$ in (9) and, hence, reformulate the problem in terms of the link trajectories, $q(t)$ which are now the only optimization variables. In other words, we have now the following simpler optimization problem:

$$\min_{\tau(t),q} J_i(q, \dot{q}, \ddot{q}), \qquad i \in \{1, 2\}$$

$$\text{s.t.} \begin{cases} \text{Dynamics equations} \\ q(t) = q(t+T) \\ \xi_1(q, \dot{q}, \ddot{q}) \leq 0 \\ \xi_2(q, \dot{q}, \ddot{q}) = 0. \end{cases} \tag{19}$$

Notice that we would like to write the new optimization problem in a conventional form, e.g., in a general Bolza form, as follows:

$$\min_{u(t)} \Phi\big(x(t_f)\big) + \int_{t_0}^{t_f} L(x(t), u(t))dt$$
$$\text{s.t.} \begin{cases} \dot{x} = g(x(t), u(t)) \\ x(0) = x_0 \\ \chi_1(x) \leq 0 \\ \chi_2(x) = 0 \end{cases} \tag{20}$$

where $\Phi(\cdot)$ and $L(\cdot)$ provide a mathematical representation of the objective function in terms of the states $x(t)$ and the control input $u(t)$; $g(\cdot)$ is a function of the system dynamics; x_0 denotes the initial conditions for the states, and χ_1 and χ_2 are the nonlinear constraints that define the task.

For example, let us consider the SEA case using the cost functional J_2. Replacing the coefficients $F_{S,j}$, $G_{S,j}$, $H_{S,j}$, and the optimal stiffness $\hat{K}_j$ (18), in the cost functional $J_{2,j}$ (18), it yields

$$\begin{aligned} J_{2,j} &= \frac{G_{S,j}^2}{4F_{S,j}} - \frac{G_{S,j}^2}{2F_{S,j}} + H_{S,j} = -\frac{G_{S,j}^2}{4F_{S,j}} + H_{S,j} \\ &= -\frac{\left[\int_0^T 2J_{m_j}\ddot{f}_j\left(J_{m_j}\ddot{q}_{d,j} + f_j\right)dt\right]^2}{4\left(\int_0^T \left(J_{m_j}\ddot{f}_j\right)^2 dt\right)} \\ &\quad + \int_0^T \left(J_{m_j}\ddot{q}_{d,j} + f_j\right)^2 dt \end{aligned}$$

which is not in the form (20).

Having the optimization problem written in the Bolza form would be useful to solve the optimal trajectory using GPOPS-II [43]. To translate the problem we propose the following steps, providing an example for an SEA using the cost index J_2.

1) Write the actuated dynamics of the system as in (7), that can be expanded as follows:

$$f = M(q)\ddot{q} + C(q, \dot{q})\dot{q} + K_v\dot{q} \tag{21}$$

which describes a planar manipulator, where $M(q)$, $C(q, \dot{q})$, and K_v, are in order the inertia, coriolis, and damping matrices; q, $\dot{q}$, and $\ddot{q}$ are the link positions, velocities, and accelerations, respectively.

2) Define a vector of augmented state variables that take into account all the system dynamics. In the SEA case of the example the dynamics are represented by (7), (8), (21), and the augmented state space vector $x(t)$ can be written as follows:

$$x(t) = \left[x_1^T, x_2^T, x_3^T, x_4^T, x_5^T, x_6^T, x_7^T, x_8^T\right]^T$$

$$\begin{bmatrix} x_1(t) \\ x_2(t) \\ x_3(t) \\ x_4(t) \\ x_5(t) \\ x_6(t) \\ x_7(t) \\ x_8(t) \end{bmatrix} = \begin{bmatrix} q \\ \dot{q} \\ \ddot{q} \\ \dddot{q} \\ \ddddot{q} \\ \int_0^t \left(J_m\ddot{f}\right)^2 dt \\ \int_0^t 2J_m\ddot{f}(J_m\ddot{q} + f)dt \\ \int_0^t (J_m\ddot{q} + f)^2 dt \end{bmatrix}.$$

Notice that in this example $x(t) \in \Re^{8n}$ as each of the eight vectors $x_1(t)..\ x_8(t)$ has n components.

3) Write the corresponding augmented state space dynamics $\dot{x} = g(x(t), u(t))$ which in this case is

$$\begin{bmatrix} \dot{x}_1 \\ \dot{x}_2 \\ \dot{x}_3 \\ \dot{x}_4 \\ \dot{x}_5 \\ \dot{x}_6 \\ \dot{x}_7 \\ \dot{x}_8 \end{bmatrix} = \begin{bmatrix} x_2 \\ x_3 \\ x_4 \\ x_5 \\ V(t) \\ \left(J_m\ddot{f}\right)^2 \\ 2J_m\ddot{f}(J_m x_3 + f) \\ (J_m x_3 + f)^2 \end{bmatrix} \tag{22}$$

where $V(t)$ is for example a piecewise continuous function,

$$\begin{aligned} f &= M(x_1)x_3 + C(x_1, x_2)x_2 + K_v x_2 \\ \ddot{f} &= \dddot{M}(x_1, x_2, x_3)x_3 + 2\ddot{M}(x_1, x_2)x_4 + \dot{M}(x_1)x_5 \\ &\quad + \ddot{C}(x_1, x_2, x_3, x_4)x_2 + 2\dot{C}(x_1, x_2, x_3)x_3 \\ &\quad + C(x_1, x_2)x_4 + K_v x_4. \end{aligned}$$

4) Write the cost functional in terms of the state variables. In this example we choose the expression of J_2, which is

$$\Phi\big(x(t_f)\big) = J_2 = \sum_{j=1}^{n} J_{2,j} = \sum_{j=1}^{n}\left(-\frac{x_{7,j}^2}{4x_{6,j}} + x_{8,j}\right)$$
$$L(x(t), u(t)) = 0. \tag{23}$$

5) Evaluate the other constraints χ_1 and χ_2 of (20), which in this case are zero.

6) Knowing the initial conditions $x(0) = x_0$, the optimal trajectories can now be solved numerically, for example by using GPOPS-II.

For all cases considered, namely, systems actuated by PEAs or by SEAs using indices J_1 or J_2, the same procedure can be followed according to the specific case, i.e., the states might be properly chosen and the formulation needs to be adapted to the dynamics of the system.

VI. Examples of Simultaneous Optimization of Stiffness and Link Trajectories

The problem in (19), after applying the methodology proposed, depends only on the trajectories. At this point, it is still an optimal control problem that can be solved, for instance, using nonlinear programming methods. Particularly, we use a general-purpose optimal control software (general pseudospectral optimization control software-GPOPS-II) to find the optimal trajectories.

As defined in [43], the optimization problem that will be solved using GPOPS-II is stated in details in the following.

1) Determine the desired task: for the example, a pick and place-like task to be executed with a two-link planar manipulator. Two points of interest are required; e.g., the starting (pick) point Q_s and the end (place) point Q_e of the end-effector, defined in the cartesian space.
2) Consider that the problem can be written in p phases, where p indicates a number of events for which one or more conditions may change. For the example, with $p = 2$; the phases are defined as follows.
   a) *Phase 1:* The motions of the system to go from Q_s to Q_e in a time interval $[0, T_1]$.
   b) *Events:* In the start and end points, joint velocity is zero.
   c) *Phase 2:* The motions of the system to go from Q_e to Q_s in a time interval $[T_1, T_2]$.
3) Write the cost function for each phase in terms of the state variables as in (23). In this case the cost function does not change for each phase.
4) Define the constraints for the desired task.
   a) Dynamic constraints, defined as $\dot{x}^{(p)} = a^{(p)}[x^{(p)}, u^{(p)}, t^{(p)}]$. For this problem, the dynamics is defined as in (22).
   b) Event constraints given by $b_{\min} \leq b[x^{(p)}, u^{(p)}, t^{(p)}, s] \leq b_{\max}$. For this problem, when the event occurs, i.e., the start or end points are achieved and the velocity of the joints becomes zero, all the states have the same value, which ensures that the trajectory is continuous.
   c) Other constraints as inequality path constraints, defined as $c_{\min} \leq c[x^{(p)}, u^{(p)}, t^{(p)}] \leq c_{\max}$ or state constraints defined as $q^{(p)}_{\min} \leq q^{(p)} \leq q^{(p)}_{\max}$. For this example, the minimum and maximum bounds that the states may achieve considering the physical characteristics of the system, and the desired initial and end points in the Cartesian space.

   Notice that the constraints defined here correspond to the constraints defined in (19).

In the following example, we analyze a two-link robot actuated by SEAs and we compute the cost when using sinusoidal trajectories (Section VI-A) and the cost when using the optimized trajectories (Section VI-B).

A. Two-Link Manipulator: Example of Stiffness Optimization

Consider now a two-link manipulator actuated by SEAs, which is, hence, an underactuated system (two motors and four DoF), whose dynamics is given by (7) and (8). Assume that $q_{1,d} = A_1 \sin(\omega t) + B_1$ and $q_{2,d} = A_2 \sin(\omega t) + B_2$ are the desired link trajectories. The robot performs a pick and place-like task on a horizontal plane, moving from a given initial position Q_1 to a given final position Q_2. For this example, several simulations are reported in [39], where it is shown that the optimization of the stiffness allows to save up to 62% of energy w.r.t. the rigid case. One particular case is presented, here, as a general example of the overall results. For this case, the desired initial and final positions of the end effector in the task space are given by the cartesian points $Q_1 = (-13; 5)$ and $Q_2 = (14; 6)$ (in centimeters). The desired link trajectories calculated by inverse kinematics are assumed to be sinusoidal at a frequency $\omega = 4.5$ rad/s and the amplitudes and bias angles are, respectively, $A_1 = 0.45$ rad, $B_1 = 1.5$ rad, $A_2 = 1.5$ rad, and $B_2 = 0.1$ rad. Table II shows the simulation results after applying the proposed method to determine the optimal stiffness for each joint with respect to J_1

TABLE II
COST INDEX J_1 (SIMULATED) FOR DIFFERENT VALUES OF STIFFNESS IN A TWO-LINK ROBOT ACTUATED BY SEAS. $\hat{K}$ IS THE OPTIMAL STIFFNESS VALUE DETERMINED FROM THE SIMULATIONS. K^* IS THE NEAREST ELASTIC CONSTANT AVAILABLE FOR THE IMPLEMENTATION. THE TRAJECTORIES OF JOINTS 1 AND 2 ARE $q_1 = 0.45\cos 4.5t + 1.5$ AND $q_2 = 1.5\cos 4.5t + 0.1$, RESPECTIVELY

	Joint 1	Joint 2	J_1 Total
$\hat{K}$ $[Nm/rad]$	0.2	0.09	
$J_1[W^2s]$	0.003	0.07	0.073
K^* $[Nm/rad]$	0.22	0.1	
$J_1[W^2s]$	0.003	0.075	0.078
K_{min} $[Nm/rad]$	0.05	0.05	
$J_1[W^2s]$	0.04	0.35	0.39
K_{max} $[Nm/rad]$	0.82	0.82	
$J_1[W^2s]$	0.07	0.1	0.17
Rigid case	$K \to \infty$	$K \to \infty$	
$J_1[W^2s]$	0.09	0.1	0.19

TABLE III
PARAMETERS USED FOR THE EXAMPLE PRESENTED, EMULATING A PICK AND PLACE TASK

Parameters	Value
$Q_s = (x_s, y_s)$	(11.25, 6.9) cm
$Q_e = (x_s, y_s)$	(-10.17, 8.42) cm
T	2π s
Initial conditions	$q_1(0) = 1.4$ rad, $q_2(0) = -1.7$ rad
Constraints (Periodic Motions)	$q_1(T/2) = 1.6$ rad, $q_2(T/2) = 1.7$ rad $q_j(0) = q_j(T)$ $\dot{q_j}(0) = \dot{q_j}(T) = \dot{q_j}(T/2) = 0$ rad/s

In this case, from the simulation we obtain $\hat{K}_1 = 0.2$ Nm/rad and $\hat{K}_2 = 0.09$ Nm/rad. We observe that for lower values of stiffness the cost reaches a maximum value. This confirms that it is not worth to use softer actuators than the optimal. The simulation results presented, here, will be useful for a more complete understanding of the problem together with the experimental results in next section.

B. Two-Link Manipulator: Example of Simultaneous Optimization of Stiffness and Trajectory

Now, for the same two-link manipulator, we define the desired cartesian points of start (Q_s) and end (Q_e) of a pick and place task and calculate the initial conditions of position and velocity for each joint to reach the desired points. Table III shows the parameters set for the example reported here.

Using the optimization software GPOPS-II, the optimal link trajectories $\hat{q}_1(t)$ and $\hat{q}_2(t)$ are obtained, as well as the optimal stiffness $\hat{K}_1$ and $\hat{K}_2$ such that they satisfy the constraints and minimize the cost functional $J_2 = J_{2,1} + J_{2,2}$. Fig. 4 shows the resulting optimal trajectories for the desired task. Notice

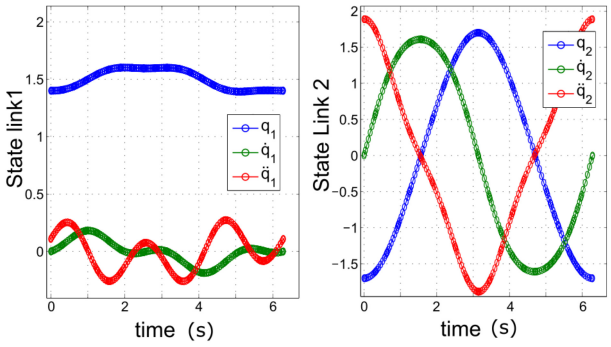

Fig. 4. Optimized link trajectories for a two-link SEA manipulator. q is the position, $\dot{q}$ is the velocity, and $\ddot{q}$ is the acceleration.

that the trajectories obtained are periodic, but they are not sinusoidal.

With the optimized trajectories and the optimal stiffness $\hat{K}_1 = 0.002$ Nm/rad and $\hat{K}_2 = 0.0001$ Nm/rad, the cost is $J_2 = 3.5 \times 10^{-4}$. Using other trajectories rather than the optimal ones, e.g., sinusoidal trajectories that satisfy the constraints, we obtain $J_2 = 4.3 \times 10^{-4}$ with $\hat{K}_1 = 0.1$ Nm/rad and $\hat{K}_2 = 0.001$ Nm/rad. This means that the optimization of the trajectories can further reduce the energy consumption. For this particular case, the reduction is of 20% w.r.t. the case when only the stiffness is optimized.

VII. Experimental Results

To show the validity and the applicability of the methodology extension proposed in this article, we report the results of experimental tests. More specifically, we present the example of a two-link robot actuated by SEAs which performs a pick and place task. We report the results when using predefined cyclic trajectories and we carry out the optimization of its link trajectories. We leave as a proposal for future work a robustness analysis and a detailed performance comparison between the state-of-the-art and the methodology extension proposed in this article.

A. Two-Link Manipulator

1) System Description: The prototype of the manipulator is represented in Fig. 5. It is an underactuated arm with two links (n. 1 in Fig. 5), the first link is composed by the parts highlighted in green, while the second by the blue part. The joints (2), are connected to the motors (3) by means of series elastic transmissions (4). Each transmission is composed by two pulleys connected by a rubber band. Either the joints and the links are provided with contactless magnetic rotary position sensors AS5045[2] (n. 5 in Fig. 5). Additionally, hall effect analog current sensors ACS714[3] have been placed in series to each motor in order to measure the current consumption during the task. An electronic board[4] is used to acquire the measurements and to implement a closed-loop position control scheme. All the position measurements acquired from the

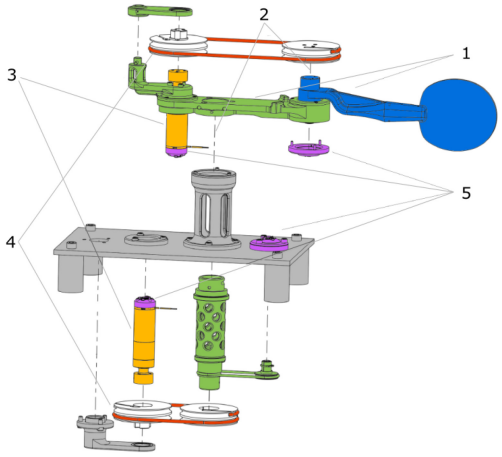

Fig. 5. Prototype of the 2 DoF manipulator actuated by SEAs. The main components are highlighted as follows: links (1); joints (2); motors (3); elastic transmissions (4); and sensors (5).

sensors have been filtered using a Butterworth lowpass filter, with cutoff frequency $\omega_c = 15$ rad/s to reduce noise effects.

2) Index Calculation: Let $\tau = K_I I$, be the torque needed to generate a motion, where K_I is the datasheet value 18.4 mN/A,[5] and I is the current measurement sampled each 5 ms. Then the cost indices can be calculated by replacing this torque τ, in (16), and (17).

Additionally, for the analysis, consider the root mean square value of the current (I_{RMS}), calculated as follows:

$$I_{\text{RMS}_j} = \sqrt{\frac{1}{T}\left(\int_{t_0}^{t_0+T} I_j^2(t)dt\right)} \tag{24}$$

which in practice is strictly related to the cost indices proposed. To implement the I_{RMS} function, the current measurements are squared and then filtered using a Butterworth lowpass filter with cutoff frequency $\omega_c = 2$ rad/s.

3) Experimental Tests: We determine the optimal spring constant for each joint by applying the methodology proposed. To implement the optimal stiffness, we characterize different elastic elements (series elastic transmissions) using a Materials Testing Machine.[6] Thus, we obtain the curve of the force versus the displacement $F = -k\Delta(x)$ for each elastic rubber band. The elastic elements used are approximately linear, so we can calculate the elastic constant k (in N/m). Fig. 6-left shows the characteristic curve of one of the elastic rubbers having length $L = 16$ cm. A force is applied at constant speed to elongate it up to 2 cm, and the cycle is repeated several times for each trial. With a linear regression method we obtain $k = 640$ N/m. Fig. 6-right shows the characteristic curve of a softer elastic band. Notice that the curve has a linear region, which is considered for the analysis; although the rubber bands characteristic is assumed approximately linear, nonlinearities exist and must be checked during the experiments since their effect can be significant [44]. For example, the measurement of the hysteresis shown in Fig. 6 yields a value of 41.4 mJ/cycle for the stiffer elastic band and 4.47 mJ/cycle for the softer elastic

[2]http://www.ams.com
[3]http://www.pololu.com/file/0J196/ACS714-Datasheet.pdf
[4]http://www.naturalmotioninitiative.com/

[5]http://dcx.maxonmotor.com Maxon motor DCX 22S 24V with graphite brushes and planetary gearhead, reduction ratio 186:1
[6]Zwick Roell Z005.

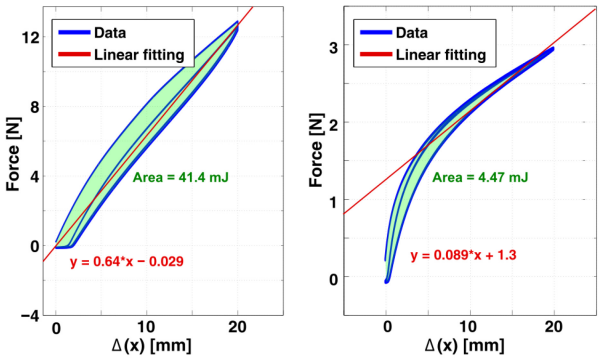

Fig. 6. Characteristic curves of force versus displacement of the elastic elements.

band. Reducing this hysteresis could lead to increased energy savings in our test setup [4].

The pulleys of the platform allow to change the linear elastic constant into the corresponding torsional elastic constant: $K_t = kr^2$ (in Nm/rad), where r is the pulley radius. For instance, with a pulley of $r = 3$ cm, the torsional elastic constant for the stiffer sample is $K_t = 0.57$ Nm/rad. Using different pulley radius and different elastic elements, we can have different spring values as well. Notice that the torsional constants can be calculated with good accuracy. It is possible to estimate the error on the torsional spring constant $\mathcal{E}_{K_t}$ by evaluating the expression $(K_t + \mathcal{E}_{K_t}) = (k + \mathcal{E}_k)(r + \mathcal{E}_r)^2$, Since the worst-case error in determining the linear constant, is $\mathcal{E}_k \approx \pm 62$ N/m and since the error on the radius of the 3-D-printed pulleys[7] is $\mathcal{E}_r \approx \pm 1$ mm, we obtain $\mathcal{E}_{K_t} \approx 0.1$ Nm/rad $\approx \pm 17\% K_t$. However, the available values depend on the materials and on the pulleys used. Based on these calculations, for the implementation we consider $\hat{K} \pm 10\%$. The differences between the costs when using the theoretical optimal values and the implemented values of stiffness do not change significantly in simulation (around 1% as shown in Table II). For the experiments carried out, we have used five different rubber bands and pulleys of two different radii ($r = 2$ cm and $r = 3$ cm).

The experiments have been carried out to accomplish a repetitive task, as a pick-and-place task, where the end effector moves cyclically from one initial position Q_1 to a certain final position Q_2, which are defined previously. There are two interesting cases for this study that will be considered, namely, predefined link trajectories to accomplish the desired task, and optimized link trajectories.

4) Stiffness Optimization of Two-DoF Manipulator With Predefined Trajectory: Consider now the case of stiffness optimization of the two-link manipulator with predefined trajectory. Assume a simple case of cyclic trajectory, defined for each link as $q_j = A_j \cos \omega t + B_j$, where the frequency ω can be chosen according to the system specifications, and the amplitude A_j and offset angle B_j, as well as the input to the motors, i.e., θ_j, are properly calculated through inverse kinematics, considering the elastic element between the actuator and the link.

[7]Stratasys Dimension Elite.

TABLE IV
RESULTS: MEASURED INDEX J_1 AND CURRENT CONSUMPTION FOR EACH STIFFNESS CASE FOR ONE CYCLE OF THE PICK AND PLACE TASK. DISTANCE FROM THE DESIRED INITIAL $Q_1 = (-13, 5)$ AND END $Q_2 = (14, 6)$ POINTS OF THE PICK AND PLACE TASK FOR EACH CASE OF ACTUATION

	$\hat{K}$	$K < \hat{K}$	$K > \hat{K}$	Rigid
$J_{1_{TOTAL}}$	0.1542	0.7964	0.3154	0.5672
$I_{RMS_{Total}}$ (A_{rms})	1.37	2.95	1.79	1.68
K_1 [Nm/rad]	0.2	0.08	0.57	Rigid
K_2 [Nm/rad]	0.1	0.06	0.35	Rigid
Distance from Q_1 [cm]	2.8	1.9	1.1	0.9
Distance from Q_2 [cm]	3.6	1.0	1.1	0.3

Recall the simulation results reported in Section VI-A, which are used to generate the experimental trials in this section. For the particular case, the desired initial and end points of the pick-and-place task, as well as the desired trajectories are the ones presented in the simulation results in Table II. The use of elastic actuation was analyzed in four cases: first, using the implemented optimal spring values ($K_j^* \approx \hat{K}_j \pm 10\%$) for each joint $K_1^* = 0.22$ Nm/rad and $K_2^* = 0.1$ Nm/rad, calculated through the methodology presented; second, with softer springs than the optimal for each joint $K_{1_{\text{soft}}} = 0.08$ Nm/rad, $K_{2_{\text{soft}}} = 0.06$ Nm/rad; third, using an elastic element stiffer than the optimal one, $K_{1_{\text{stiff}}} = 0.57$ Nm/rad, $K_{2_{\text{stiff}}} = 0.35$ Nm/rad; and finally the rigid case. In all the studied cases, we verify that the desired joint trajectories (θ) are followed properly. The measured joint position tracks the desired joint trajectory given to the motor with a mean error of 0.1%. All the calculations have been done considering the steady state of the system. The analysis of the initial current pick consumption and transient is not in the scope of this work.

Furthermore, to ensure that the task performed is the same in all the compared cases, we verify the behavior of the corresponding link trajectories. Beyond having similar link angular positions, the comparison is done between the corresponding initial and end desired positions of the end effector Q_1 and Q_2 for each case of analysis, i.e., the task is accomplished. Table IV shows the distance between the experimental and the desired values of the initial and end positions for the same desired link trajectories using different stiffness values, namely, optimal, softer than the optimal, stiffer than the optimal, and rigid.

Fig. 7(a) and (b) show the measured link positions q_1 and q_2, respectively, for the four cases of stiffness analyzed. Observe that the softer elastic, particularly in Link 2 produces higher angular position errors and a delay.

The angular positions of Link 2 in the other cases (optimal spring, stiffer spring, and rigid actuation) behave as expected. Instead, there are bigger differences in the position of Link 1 with respect to the desired behavior. The differences in the measured link positions are mainly due to nonlinearities, nonmodeled dynamics, and uncertainties in the model.

The I_{RMS} value of each joint provides additional information to analyze the energy consumption and it is strictly related to the cost indices. We have observed that with the optimal joint stiffness the I_{RMS} is always lower than for the rest of the cases,

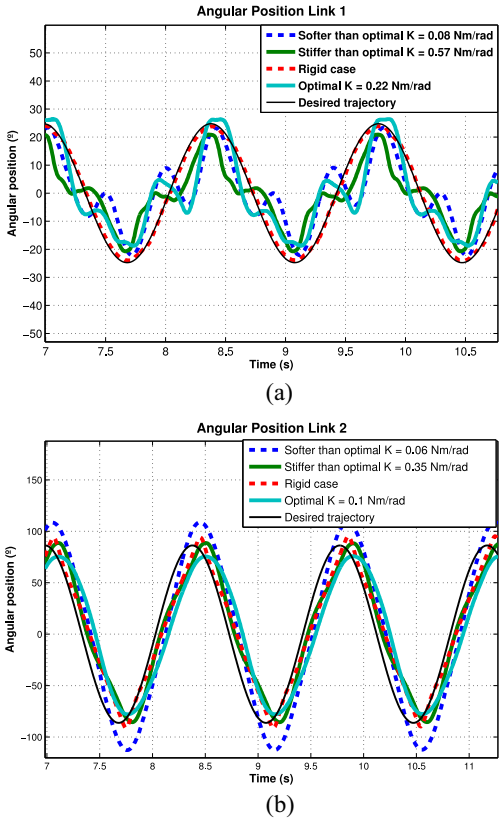

Fig. 7. Compared link positions for the same desired task. (a) Link 1. (b) Link 2.

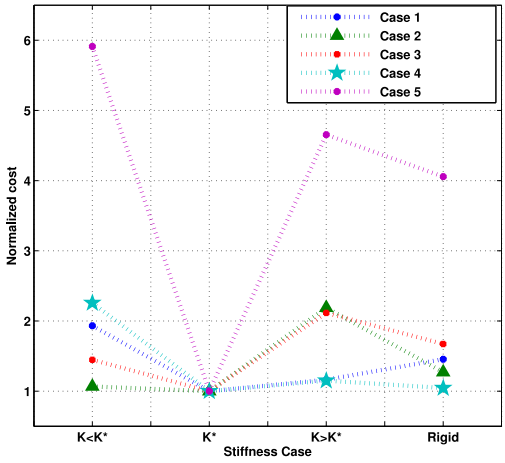

Fig. 8. Normalized actuation performance of the trajectories of Table V.

TABLE V
DIFFERENT CASES OF LINK TRAJECTORIES q_1 AND q_2 USED TO REPORT FIG. 8. COEFFICIENTS A AND B ARE IN RAD, AND FREQUENCIES ω ARE IN RAD/S

Case	q_1	q_2
1	$A_1{=}0.31\ B_1{=}1\ \omega_1{=}1$	$A_2{=}1.7\ B_2{=}0.04\ \omega_2{=}1$
2	$A_1{=}0.1\ B_1{=}1.5\ \omega_1{=}2$	$A_2{=}1.6\ B_2{=}0.01\ \omega_2{=}2$
3	$A_1{=}0.5\ B_1{=}1\ \omega_1{=}3.5$	$A_2{=}1.6\ B_2{=}0.03\ \omega_2{=}3.5$
4	$A_1{=}0.05\ B_1{=}1.6\ \omega_1{=}4$	$A_2{=}1.5\ B_2{=}0\ \omega_2{=}4$
5	$A_1{=}0.25\ B_1{=}1.5\ \omega_1{=}4.5$	$A_2{=}1.7\ B_2{=}0.1\ \omega_2{=}4.5$

proving that lower energy consumptions can be obtained with the optimization of actuation parameters. Moreover, the stiff transmission is not always the worst case in terms of energy consumption; the softer case can also be the most expensive one.

Table IV summarizes the cost results for the presented case. When using the optimal springs, the savings in terms of J_1 are at least 58% w.r.t. a stiffer case and 79% w.r.t. the rigid case. Notice that the trend is the same as expected from the simulations. The values in Table IV are calculated from the measurements, therefore, the accuracy of the index depends directly on the sensors accuracy, which for the encoders is $\theta \pm 0.002$ rad, and for the current sensors is $I \pm 1$ mA. The error on the cost index $\mathcal{E}_{J_1}$ can be computed by evaluating the equation $(J_1 + \mathcal{E}_{J_1}) \propto (I + \mathcal{E}_I)^2(\dot{\theta} + \mathcal{E}_{\dot{\theta}})^2$, assuming as reference values $\dot{\theta} = 9$ rad/sec and $I = 1$ A, thus, obtaining $\mathcal{E}_{J_1} \approx \pm 0.24\% J_1$, which is accurate for our purpose.

In general, a significant energy saving is achieved when optimizing the actuation parameters. In the following, we present some consolidated results from a set of experiments. We carried out 320 trials of the same task using different elastic transmissions and different trajectories at different frequencies as summarized in Table V. Fig. 8 shows the costs of this repetitive task when using the optimal stiffness rather that softer, stiffer, or rigid actuation. We chose different desired trajectories at different frequencies from the 320 trials performed, as summarized in Table V. In each case, the cost of the task was calculated when the system has reached the steady state. For the analysis, the cost J is normalized in every case with respect to the cost of when using the optimal actuation parameters, such that for the latter, the normalized cost is $J_n = 1$. Furthermore, notice that for all the other cases of stiffness, the cost is always higher than when optimizing the stiffness. Depending on the frequency and on the amplitude of the desired trajectories, the optimized stiffness allows energy savings up to 79%.

5) Simultaneous Optimization of Link Trajectories and Stiffness of Two-Link Manipulator With SEAs:

Herein, we present the case of simultaneous optimization of joint trajectories and stiffness of a two-link manipulator with SEAs. In this part, the results reported correspond to a set of experiments carried out to test the optimal trajectories and stiffness found by solving the problem with GPOPS-II as described in Section VI. In order to compare the results with the previous case of predefined trajectories, the conditions of the experiments are the same; the initial and end points (Q_1; Q_2) of the task are the ones chosen before. The desired states of the links are shown in Fig. 9. The optimal joint stiffness for this example is $\hat{K}_1 = 0.12$ Nm/rad and $\hat{K}_2 = 0.05$ Nm/rad. Recall results on Table IV. Now, Table VI shows the distance between the experimental and the desired values of the initial and end positions when using the optimal stiffness and optimal joint trajectories. On the other hand, regarding the cost index, observe that the mean square value of the current spent is $I_{\mathrm{RMS}_{\mathrm{Total}}} = 1.09\ A_{\mathrm{rms}}$ and the index $J_1 = 0.12$ which is approximately a 20% lower consumption than the optimal case when using a predefined sinusoidal trajectory, under the same conditions.

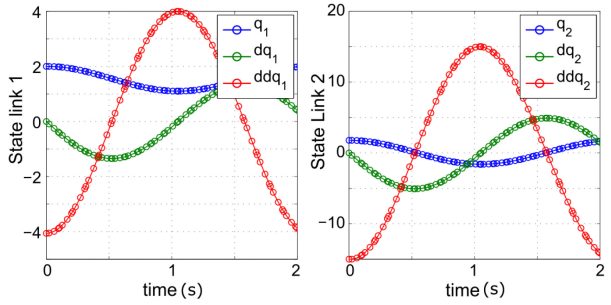

Fig. 9. Optimization of trajectories: desired steady states trajectories for the manipulator's links state. $q_1 = 0.44\cos(3t) + 1.5$ and $q_2 = 1.65\cos(3t)$.

TABLE VI
RESULTS: INDEX AND CURRENT CONSUMPTION FOR ONE CYCLE OF THE PICK AND PLACE TASK

	with $\hat{q_j}$ and $\hat{K}$
$J_{1_{TOTAL}}$	0.12
$I_{RMS_{Total}}$ (A_{rms})	1.09
K_1 [Nm/rad]	0.12
K_2 [Nm/rad]	0.05
Distance from Q_1 [cm]	1.02
Distance from Q_2 [cm]	1.8

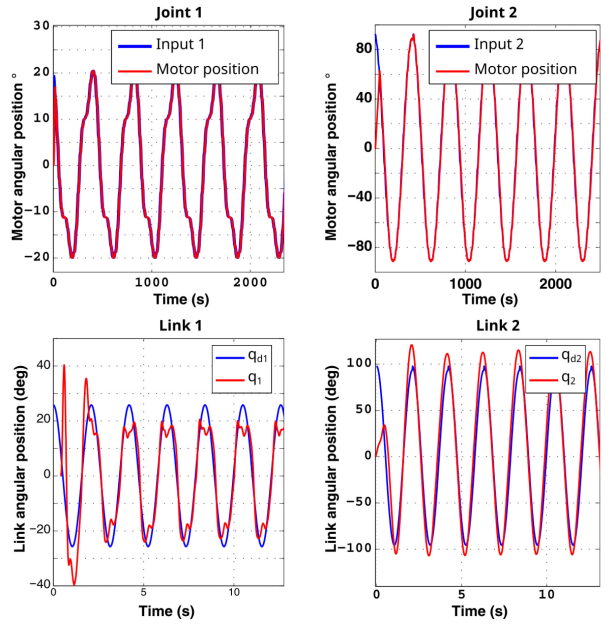

Fig. 10. Joints (top) and links (bottom) angular positions, measured versus desired.

Fig. 10-top shows that the joints track the angular position and achieve a steady state. Fig. 10-bottom shows the measured link positions q_1 (left) and q_2 (right) compared to the desired trajectories given by the optimization process in GPOPS-II. Due to the nonlinear behavior of the elastic elements, particularly the one of Link 1, the angular position presents a periodic error. However, the behavior of the system in terms of the initial and end points of the end-effector is not significantly affected, achieving the task.

VIII. CONCLUSION

In this article, we extended the methodology proposed in [39] in order to determine the optimal actuation parameters that minimizes a cost functional based on energy consumption.

We considered well-known tasks, mainly cyclic, as the pick-and-place, to gain insight in the role of elastic actuation for reducing the energy cost during the motion. The results obtained can be applied directly to more complex systems such as hopping robots for which soft actuation can be exploited to achieve a reduction of the energy cost.

Also, we have shown that the trajectories to accomplish a task play an important role. The problem of simultaneously optimizing the trajectories and the actuation parameters is complex because these variables are highly coupled. Thus, to solve this problem, the optimization problem was cast in a simpler one that regards only the link trajectories. To solve the trajectory problem, there are some parameters that are needed a priori, namely, the period or the total duration of the task; the frequency of the motion; the mechanical constraints; the initial and final position of the links and any point reached by the link.

Several simulations and some experimental tests were carried out to show the validity of the methodology extension proposed in this article. The strength point of our work is the fact that, thanks to our extended methodology, it is possible to decouple complex problems in which it is needed to concurrently optimize the actuation parameters and the link trajectories, providing an analytical solution to the optimization problem. We are also able to show that using the optimal actuation parameters the savings obtained go up to 62% with respect to a rigid actuation and further savings of at least 20% are obtained when optimizing simultaneously the actuation parameters and the link trajectories.

REFERENCES

[1] "United Nations 2030 agenda, sustainable development goals." Accessed: Jan. 5, 2022. [Online]. Available: sdgs.un.org/goals

[2] N. Barnett, D. Costenaro, and I. Rohmund, *Direct and Indirect Impacts of Robots on Future Electricity Load*, ACEEE Summer Study Energy Efficiency Ind., Washington, DC, USA, 2017.

[3] G. Carabin, E. Wehrle, and R. Vidoni, "A review on energy-saving optimization methods for robotic and automatic systems," *Robotics*, vol. 6, no. 4, p. 39, Dec. 2017.

[4] G. Grandesso, G. Bravo-Palacios, P. M. Wensing, M. Fontana, and A. D. Prete, "Exploring the limits of a redundant actuation system through co-design," *IEEE Access*, vol. 9, pp. 56802–56811, 2021.

[5] R. V. Ham, T. Sugar, B. Vanderborght, K. W. Hollander, and D. Lefeber, "Compliant actuator designs," *IEEE Robot. Autom. Mag.*, vol. 16, no. 3, pp. 81–94, Sep. 2009.

[6] J. Ackerman and J. Seipel, "Energetics of bio-inspired legged robot locomotion with elastically-suspended loads," in *Proc. IEEE/RSJ Int. Conf. Intell. Robots Syst. (IROS)*, 2011, pp. 203–208.

[7] B. Vanderborght et al., "Exploiting natural dynamics to reduce energy consumption by controlling the compliance of soft actuators," *Int. J. Robot. Res.*, vol. 25, no. 4, pp. 343–358, 2006.

[8] K. Sreenath, H. W. Park, I. Poulakakis, and J. W. Grizzle, "A compliant hybrid zero dynamics controller for stable, efficient and fast bipedal walking on MABEL," *Int. J. Robot. Res.*, vol. 30, no. 9, pp. 1170–1193, 2011.

[9] N. Schmit and M. Okada, "Optimal design of nonlinear springs in robot mechanism: Simultaneous design of trajectory and spring force profiles," *Adv. Robot.*, vol. 27, no. 1, pp. 33–46, Feb. 2013.

[10] A. R. Ghiasi, G. Alizadeh, and M. Mirzaei, "Simultaneous design of optimal gait pattern and controller for a bipedal robot," *Multibody Syst. Dyn.*, vol. 23, pp. 401–429, Apr. 2010.
[11] A. Liu, H. Liu, B. Yao, W. Xu, and M. Yang, "Energy consumption modeling of industrial robot based on simulated power data and parameter identification," *Adv. Mech. Eng.*, vol. 5, no. 10, pp. 1–11, 2018.
[12] M. Catalano et al., "VSA-CubeBot: A modular variable stiffness platform for multiple degrees of freedom robots," in *Proc. IEEE Int. Conf. Robot. Autom. (ICRA)*, 2011, pp. 5090–5095.
[13] M. D. Taylor, "A compact series elastic actuator for bipedal robots with human-like dynamic performance," M.S. thesis, Robot. Inst., Carnegie Mellon Univ., Pittsburgh, PA, USA, Aug. 2011.
[14] A. Albu-Schaffer et al., "Soft robotics," *IEEE Robot. Autom. Mag.*, vol. 15, no. 3, pp. 20–30, Sep. 2008.
[15] N. G. Tsagarakis, M. Laffranchi, B. Vanderborght, and D. Caldwell, "A compact soft actuator unit for small scale human friendly robots," in *Proc. IEEE Int. Conf. Robot. Autom. (ICRA)*, 2009, pp. 4356–4362.
[16] G. A. Pratt and M. M. Williamson, "Series elastic actuators," in *Proc. IEEE/RSJ Int. Conf. Intell. Robots Syst. (IROS) Human Robot Interact. Cooperative Robots*, Aug. 1995, pp. 399–406.
[17] M. G. Catalano et al., "A variable damping module for variable impedance actuation," in *Proc. Int. Conf. Robot. Autom.*, Saint Paul, MN, USA, 2012, pp. 2666–2672.
[18] J. J. Park, S. Haddadin, J. B. Song, and A. Albu-Schaffer, "Designing optimally safe robot surface properties for minimizing the stress characteristics of human-robot collisions," in *Proc. IEEE Int. Conf. Robot. Autom. (ICRA)*, 2011, pp. 5413–5420.
[19] M. Garabini, A. Passaglia, F. Belo, P. Salaris, and A. Bicchi, "Optimality principles in variable stiffness control: The VSA hammer," in *Proc. IEEE/RSJ Int. Conf. Intell. Robots Syst. (IROS)*, 2011, pp. 3770–3775.
[20] T. Verstraten, P. Beckerle, R. Furnémont, G. Mathijssen, B. Vanderborght, and D. Lefeber, "Series and parallel elastic actuation: Impact of natural dynamics on power and energy consumption," *Mech. Mach. Theory*, vol. 102, pp. 232–246, May 2016.
[21] T. Verstraten, "New actuation paradigms with high efficiency for variable load at varying speed," Ph.D. dissertation, Dept. Mech. Eng., Vrije Universiteit Brussel, Brussels, Belgium, Mar. 2018.
[22] S. A. Migliore, L. H. Ting, and S. P. DeWeerth, "Passive joint stiffness in the hip and knee increases the energy efficiency of leg swinging," *Auton. Robots*, vol. 29, no. 1, pp. 119–135, 2010.
[23] T. Schauss, M. Scheint, M. Sobotka, W. Seiberl, and M. Buss, "Effects of compliant ankles on bipedal locomotion," in *Proc. Int. Conf. Robot. Autom. (ICRA)*, 2009, pp. 2761–2766.
[24] Y. Yesilevskiy, Z. Gan, and C. D. Remy, "Energy-optimal hopping in parallel and series elastic one-dimensional monopeds," *J. Mech. Robot.*, vol. 10, Jun. 2018, Art. no. 31008.
[25] T. Exley and A. Jafari, "Maximizing energy efficiency of variable stiffness actuators through an interval-based optimization framework," *Sens. Actuat. A, Phys.*, vol. 332, Sep. 2021, Art. no. 113123.
[26] M. Scheint, M. Sobotka, and M. Buss, "Compliance in gait synthesis: Effects on energy and gait," in *Proc. 8th IEEE-RAS Int. Conf. Humanoid Robots*, 2008, pp. 259–264.
[27] L. Consolini, O. Gerelli, C. Guarino Lo Bianco, and A. Piazzi, "Minimum-time control of flexible joints with input and output constraints," in *Proc. IEEE Int. Conf. Robot. Autom.*, 2007, pp. 3811–3816.
[28] L. Consolini and O. Gerelli, "An algorithm for minimum-time feedforward control based on convexity," in *Proc. IEEE Conf. Decis. Control*, 2007, pp. 4767–4772.
[29] M. Keppler and A. De Luca, "On time-optimal control of elastic joints under input constraints," in *Proc. IEEE Conf. Decis. Control (CDC)*, 2020, pp. 4149–4156.
[30] C. Guo, H. Gao, F. Ni, and H. Liu, "A vibration suppression method for flexible joints manipulator based on trajectory optimization," in *Proc. IEEE Int. Conf. Mechatronics Autom.*, 2016, pp. 338–343.
[31] A. Palleschi et al., "Time-optimal trajectory planning for flexible joint robots," *IEEE Robot. Autom. Lett.*, vol. 5, no. 2, pp. 938–945, Apr. 2020.
[32] A. Zhakatayev, M. Rubagotti, and H. Atakan Varol, "Time-optimal control of variable-stiffness-actuated systems," *IEEE/ASME Trans. Mechatronics*, vol. 22, no. 3, pp. 1247–1258, Jun. 2017.
[33] C. Ji, M. Kong, and R. Li, "Time-energy optimal trajectory planning for variable stiffness actuated robot," *IEEE Access*, no. 7, pp. 14366–14377, 2019.
[34] L. C. Visser, S. Stramigioli, and A. Bicchi, "Embodying desired behavior in variable stiffness actuators," *IFAC Proc.*, vol. 44, no. 1, pp. 9733–9738, 2011.
[35] G. M. Gasparri et al., "Efficient walking gait generation via principal component representation of optimal trajectories: Application to a planar biped robot with elastic joints," *IEEE Robot. Autom. Lett.*, vol. 3, no. 3, pp. 2299–2306, Jul. 2018.
[36] J. W. Hurst, "The role and implementation of compliance in legged locomotion," Ph.D. dissertation, Robotics Inst., Carnegie Mellon Univ., Pittsburgh, PA, USA, 2008.
[37] N. Schmit and M. Okada, "Simultaneous optimization of robot trajectory and nonlinear springs to minimize actuator torque," in *Proc. IEEE Int. Conf. Robot. Autom. (ICRA)*, 2012, pp. 2806–2811.
[38] R. Chaichaowarat, J. Kinugawa, and K. Kosuge, "Cycling-enhanced knee exoskeleton using planar spiral spring," in *Proc. IEEE/EMBS Annu. Int. Conf.*, San Francisco, CA, USA, 2018, pp. 3206–3211.
[39] A. Velasco, G. M. Gasparri, M. Garabini, L. Malagia, P. Salaris, and A. Bicchi, "Soft-actuators in cyclic motion: Analytical optimization of stiffness and pre-load," in *Proc. 13th IEEE-RAS Int. Conf. Humanoid Robots (Humanoids)*, San Francisco, CA, USA, Oct. 2013, pp. 354–361.
[40] R. Tedrake. "Underactuated robotics—Algorithms for walking, running, swimming, flying, and manipulation." Accessed: May 26, 2022. [Online]. Available: underactuated.mit.edu
[41] M. W. Spong, "Underactuated mechanical systems," in *Control Problems in Robotics and Automation*, vol. 230. Heidelberg, Germany: Springer-Verlag, 1998, pp. 135–150.
[42] M. W. Spong, "Modeling and control of elastic joint robots," *J. Dyn. Syst., Meas., Control*, vol. 109, no. 4, pp. 310–318, Dec. 1987.
[43] A. V. Rao et al., "Algorithm 902: GPOPS, a MATLAB software for solving multiple-phase optimal control problems using the Gauss pseudospectral method," *ACM Trans. Math. Softw.*, vol. 37, no. 2, pp. 1–39, Apr. 2010.
[44] R. Chaichaowarat, J. Kinugawa, A. Seino, and K. Kosuge, "A spring-embedded planetary-geared parallel elastic actuator," in *Proc. IEEE/ASME Int. Conf. Adv. Intell. Mechatronics*, 2020, pp. 952–959.

Alexandra Velasco Vivas received the master's degree in electronics engineering from Javeriana University, Bogotá, Colombia, in 2011, and the Ph.D. degree in robotics, automation, and bioengineering from the University of Pisa, Pisa, Italy, in 2015.

She is an Electronic Engineer. She is currently an Assistant Professor with the Mechatronics Department, Universidad Militar Nueva Granada, Bogotá. Her main research areas are in control and robotics focused on rehabilitation systems, trajectory planning, and optimization.

Antonello Cherubini graduated in mechanical engineering from the Politecnico di Milano, Milan, Italy, in 2012, and the Ph.D. degree in robotics from the Sant'Anna University of Pisa, Pisa, Italy, in 2017.

He is currently an Assistant Professor (RTDA) with the University of Trento, Trento, Italy. He has been a Visiting Research Fellow with TU Delft, Delft, The Netherlands, and a Visiting Professor with the University Carlos III of Madrid, Getafe, Spain.

Dr. Cherubini's Ph.D. thesis won the Prize Bernardo Nobile.

Manolo Garabini (Member, IEEE) graduated in mechanical engineering and the Ph.D. degree in robotics from the University of Pisa, Pisa, Italy, in 2010 and 2014, respectively.

He is currently employed as an Assistant Professor with the University of Pisa. He contributed to the realization of modular variable stiffness actuators. His main research interests are in the design, planning, and control of soft and adaptive robots, from actuators to end-effectors (hands, grippers, and feet), to complex multi-dof systems.

Paolo Salaris received the M.Sc. degree in electrical engineering and the Ph.D. degree in automation and bioengineering from the University of Pisa, Pisa, Italy, in 2007 and 2011, respectively.

He has been Visiting Scholar with the Beckman Institute for Advanced Science and Technology, University of Illinois at Urbana-Champaign, Champaign, IL, USA, in 2009. He was a Postdoctoral Fellow with the Research Center "E. Piaggio," University of Pisa, from March 2011 to January 2014 and also with LAAS-CNRS, Toulouse, France, from February 2014 to July 2015. From 2015 to 2019, he was a Permanent Researcher (CRCN) with Inria Sophia Antipolis Mediterranee, Valbonne, France, and from 2019 to 2022 as an Assistant Professor with the University of Pisa, and since 2022, he has been an Associate Professor. His main research interests are optimal motion planning and control, active sensing, optimal sensors placements and optimal estimation, and multirobot and nonholonomic systems.

Antonio Bicchi graduated in mechanical engineering from the University of Pisa, Pisa, Italy in 1984.

He was a Postdoctoral Scholar with M.I.T. Artificial Intelligence Lab, Cambridge, MA, USA. He is a Professor of Robotics with the University of Pisa, Pisa, Italy, and the Senior Scientist with the Italian Institute of Technology (IIT), Genoa, Italy. He teaches Robotics and Control Systems with the Department of Information Engineering, University of Pisa. He has been leading the Robotics Group with the Research Center "E. Piaggio," University of Pisa since 1990. He is the Head of the Soft Robotics Lab for Human Cooperation and Rehabilitation, IIT. Since 2013, he has been serving as the Adjunct Professor with the School of Biological and Health Systems Engineering, Arizona State University, Tempe, AZ, USA.